VIP Adsorption Very Important Paper

International Edition: DOI: 10.1002/anie.201813517
German Edition: DOI: 10.1002/ange.201813517

Comparative Adsorption of Acetone on Water and Ice Surfaces

Jenée D. Cyran, Ellen H. G. Backus,* Marc-Jan van Zadel, and Mischa Bonn**

Abstract: *Small organic molecules on ice and water surfaces are ubiquitous in nature and play a crucial role in many environmentally relevant processes. Herein, we combine surface-specific vibrational spectroscopy and a controllable flow cell apparatus to investigate the molecular adsorption of acetone onto the basal plane of single-crystalline hexagonal ice with a large surface area. By comparing the adsorption of acetone on the ice/air and the water/air interface, we observed two different types of acetone adsorption, as apparent from the different responses of both the free O–H and the hydrogen-bonded network vibrations for ice and liquid water. Adsorption on ice occurs preferentially through interactions with the free OH group, while the interaction of acetone with the surface of liquid water appears less specific.*

Interactions of trace gases with ice and water surfaces play a major role in atmospheric chemistry. The chemical and photochemical processes of trace gases adsorbed on ice surfaces are relevant for ozone depletion and alter the chemical composition of the atmosphere. Trace gases, both inorganic and organic, are found in small quantities in the atmosphere yet have a major impact on the ozone layer.[1,2] In the troposphere, there are significantly more small oxygenated organic compounds, originating from anthropogenic emissions or products from photochemical reactions, than non-oxygenated species.[1]

Acetone is a typical small oxygenated organic molecule found in the troposphere, and a critical contributor to the formation of HO_x radicals.[2] Owing to its atmospheric relevance, acetone interacting with ice has been studied for decades, for instance by mass spectrometry[3–6] and X-ray absorption spectroscopy.[7] Mass spectrometry has been used to quantify the kinetics of acetone adsorption on ice and has provided evidence that adsorption is reversible. However, these gas-phase studies do not provide molecular-level details on the adsorption of acetone, or on how its adsorption affects the ice and water surfaces. Water is present in both forms in the troposphere, and the reactions of small organic molecules on water and ice can be very different.[8,9] A simulation study has concluded that the acetone molecule lies almost parallel to the ice surface because of two interactions; a strong interaction between the carbonyl oxygen atom and a hydrogen atom from free OH groups terminating the ice surface and weaker interactions between the methyl groups and oxygen atoms from the ice surface.[7] Little is known about the structure of acetone on water. The interaction of acetone with the water/ice OH groups could affect the OH stretching frequencies, which, in the absence of aromatic moieties in the organic molecule, are relevant for photochemical reactions via vibrational overtone pumping.[10,11] In particular, decarboxylation of malonic acid was shown to occur through a change in protonation from the aldehyde to the second carbonyl group with water acting as a catalyst.[12] Despite the relevance for the atmospheric impact of anthropogenic emissions or photochemical reactions, neither the adsorption geometry nor the vibrational frequencies have been experimentally determined.

Herein, we examine the adsorption of acetone on surfaces of ice and water by sum frequency generation (SFG) spectroscopy. Molecular-level details of the ice/air[13–16] and water/air[17–20] interfaces had previously been obtained utilizing SFG spectroscopy, revealing the structure and vibrational frequencies of the outermost surface molecules. The vibrational SFG experiments have an infrared beam in resonance with molecular vibrations to probe the arrangement of specific interfacial molecules. Here, we directly observed the adsorption of acetone onto the surfaces by monitoring the C–H stretching vibrations, and furthermore report changes to the interfacial water molecules through the O–H stretching vibrations upon acetone adsorption.

For the study of acetone interacting with the water surface, we employed different molar concentrations of acetone in water at 0 °C, contained in a Teflon container. For studying the interaction of acetone with ice, a homebuilt flow cell enabled a controlled flow of acetone vapor over the ice surface. The flow cell was placed on a copper cooling plate, illustrated in Figure 1 a, to keep the temperature of the ice at −30 °C. The gas flows over the ice surface, a single-crystalline, hexagonal ice (Ih) sample, with its basal plane exposed.[15]

To begin the ice measurements, cooled nitrogen gas (ca. 0 °C) was passed through the sample cell at a rate of 2 L h^{-1} for 30 min. The SFG spectrum in Figure 2 a shows one band in the spectral region from 2800 to 3400 cm^{-1}, which originates from hydrogen-bonded O–H stretching vibrations. To vapor-deposit acetone on the ice surface, acetone (50 μL) was placed

[*] Dr. J. D. Cyran, Prof. E. H. G. Backus, M.-J. van Zadel, Prof. M. Bonn
Molecular Spectroscopy Department
Max Planck Institute for Polymer Research
Ackermannweg 10, 55128 Mainz (Germany)
E-mail: cyran@mpip-mainz.mpg.de
backus@mpip-mainz.mpg.de
bonn@mpip-mainz.mpg.de
Prof. E. H. G. Backus
Department of Physical Chemistry
University of Vienna
Währinger Strasse 42, 1090 Vienna (Austria)
The ORCID identification number(s) for the author(s) of this article can be found under:
https://doi.org/10.1002/anie.201813517.

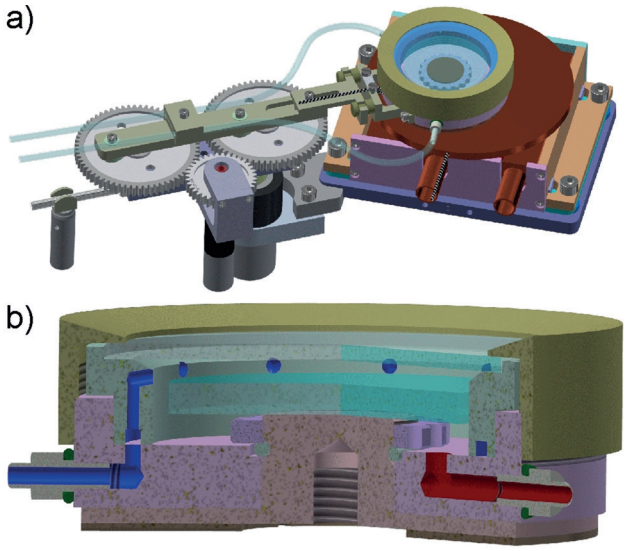

Figure 1. a) The custom-made measurement cell and cold stage for SFG experiments. b) Cross-sectional view of the sample cell. The gas flows into the cell (blue-colored inlet) and is distributed from ten different ports slightly above the ice surface (blue-colored holes, depicted larger here for clarity). The gas exits the cell under the ice through the red-colored port.

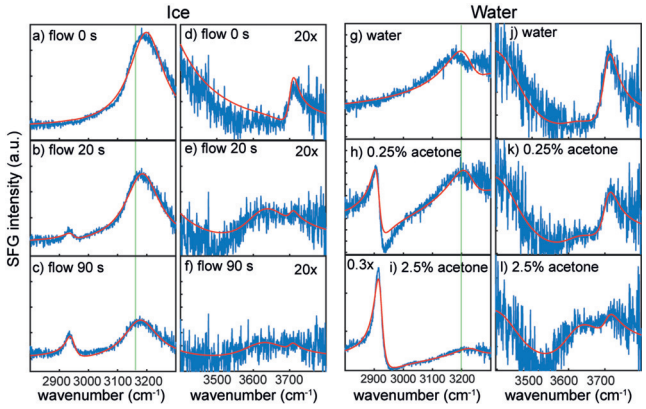

Figure 2. SFG spectra (blue) for acetone on a–f) ice and g–l) water surfaces in two different spectral regions. The 2800–3300 and the 3400–3800 cm^{-1} data sets were recorded in separate runs. The data were fit (red lines) with Lorentzian line shapes. The vertical green lines illustrate the shift in the O–H stretching vibration. For the ice spectra, the region from 3400–3800 cm^{-1} is multiplied by 20 to match the intensity of the 2800–3000 cm^{-1} spectra. Likewise, the spectrum for 2.5% acetone is multiplied by 0.3 for the 2800–3300 cm^{-1} region (i) to match the spectrum in the spectral region from 3400–3800 cm^{-1}.

in an air-tight container, which was immersed in a cold bath maintained at 0 °C. Cooled nitrogen gas was passed through the container and acted as a carrier gas for the acetone. The mixture of acetone and nitrogen flowed at a rate of 2 L h^{-1} for a defined period of time, before an SFG spectrum was collected. This process was repeated to observe the accumulation of acetone on the ice surface. Representative spectra for 20 s and 90 s flow are shown in Figure 2b and Figure 2c, respectively. The spectral feature at about 2940 cm^{-1}, corresponding to a C–H symmetric stretching vibration,[21–23] appeared and increased in intensity as more acetone was adsorbed on the ice surface. Although the clathrate hydrate of acetone can be formed under these conditions,[24] these hydrates are centrosymmetric and thus not SFG active. The increase in the signal with acetone dosage therefore shows that hydrate formation is not dominant. The O–H stretching vibration changed substantially, as illustrated in Figure 2a–c for the spectral region from 3000 to 3300 cm^{-1} and in Figure 2d–f for the spectral region from 3400 to 3800 cm^{-1}. First of all, the free OH intensity, originating from OH groups at the surface with the hydrogen atoms pointing into the air, is almost completely gone after 20 s of exposure (Figure 2e), while the CH mode continues to increase in intensity after that time. This observation is consistent with acetone preferentially interacting with the surface free OH groups.[7] The strong hydrogen bonded response of ice around 3200 cm^{-1} decreases in amplitude and shifts to lower frequencies, upon adsorption of acetone on the ice surface, indicating a strengthening of interfacial water-water hydrogen bonds.

Comparing the results of the adsorption of acetone on the ice surface with the water surface, a qualitatively different response is observed with increasing acetone concentration (Figure 2g–l). The decrease in the free OH intensity occurs more gradually, and there is some remaining free OH intensity even for a 2.5% acetone solution, which exhibits a very large CH intensity. In the hydrogen-bonding region, the lower frequency feature of the 3200/3400 cm^{-1} peak pair[17–20] shifts to slightly higher frequencies upon increasing the acetone content, which is indicative of a weakening of interfacial water–water hydrogen bonds.

For both ice and water, the addition of acetone to the surface results in the appearance of a broad peak at approximately 3600 cm^{-1}, which is most clearly visible in the 20 s flow spectrum (Figure 2e) for ice and the 2.5% acetone in water spectrum (Figure 2l). The 3600 cm^{-1} peak has been previously observed in bulk IR spectra of acetone/water mixtures[25,26] and is typical for water interacting with a carbonyl group.[27–29] Here, the decrease in the free OH intensity upon addition of acetone to the surface indicates that the free OH moieties interact with the oxygen atoms of acetone, shifting the free OH frequency from approximately 3700 to 3600 cm^{-1}.

To quantify these effects, the spectra were analyzed using the standard description of the SFG intensity as a sum of Lorentzian line shapes and a non-resonant contribution [Eq. (1)]:

$$I_{SF} \propto \left| A_{NR} e^{i\varphi_{NR}} + \sum_n \frac{A_n}{\omega_{IR} - \omega_n + i\Gamma_n} \right|^2 \quad (1)$$

A_n, ω_n, and Γ_n are the amplitude, frequency, and damping factor of the nth vibrational resonance, respectively. The non-resonant contribution $A_{NR}e^{i\varphi_{NR}}$ consists of an amplitude A_{NR} and phase φ_{NR}, where $\varphi_{NR} = 0$ for all fits. Recently, there has been a discrepancy in the literature for the sign of the hydrogen-bonded O–H stretching mode of ice.[16,30] The best

description of the ice spectra presented here was obtained using a positive peak for the hydrogen-bonded O–H stretching mode[30] and a positive peak for the free O–H stretching mode, indicating that the hydrogen atoms are pointing away from the surface into air. It should be noted that, regardless of the sign of the O–H stretching mode, the shifts in the O–H stretching modes are already apparent from the raw data. For the other bands in the ice/acetone SFG spectra, the C–H symmetric stretch and the 3600 cm^{-1} peak were each best fit with a positive peak. For water, the modes of the C–H symmetric stretch and the hydrogen-bonded O–H stretch were negative, while the 3600 cm^{-1} peak and the free O–H stretching modes were positive. The negative CH_3 symmetric stretch indicates that the acetone hydrogen atoms point up towards the air surface, as has been seen at water/air interfaces in the presence of a surfactant.[31,32]

The magnitude of the amplitudes for the C–H symmetric stretch and the different O–H stretching vibrations from the fits are plotted in Figures 3, in addition to the center frequency of the hydrogen-bonded OH stretch. For both interfaces, the CH amplitude increases with the addition of acetone (Figure 3 a, b). For ice, half of the maximum CH signal (with the maximum CH signal presumably corresponding to a coverage of one monolayer) is reached after approximately 40 s; for water, this occurs at a mole fraction of 0.75 % acetone. The exposure to acetone was chosen for both systems to reach saturation coverage, which is clear from the plateau at high concentration or long exposure times.

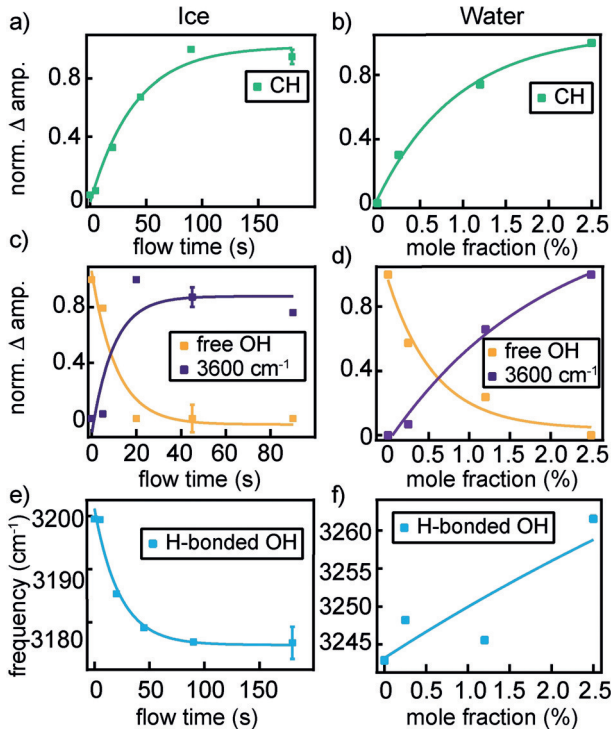

Figure 3. Extracted amplitudes and peak positions for ice and water. The normalized change in the amplitudes of the CH symmetric stretch mode (green) are plotted for a) ice and b) water. The normalized change in the amplitudes of the 3600 cm^{-1} O–H mode (purple) and the free O–H stretch mode (orange) are plotted for c) ice and d) water. Peak positions of the hydrogen-bonded water response for acetone on the e) ice and f) water surfaces. The intensities between panels cannot be compared. All data sets were fit to a single exponential function (shown as lines). Representative error bars are shown for the data, and were calculated from multiple data sets.

The amplitudes of the free O–H and the 3600 cm^{-1} O–H vibrational modes are shown in Figure 3 c and 3 d. For both ice and water, the addition of acetone triggers the free OH intensity to decrease, and the response of weakly hydrogen-bonded O–H molecules at 3600 cm^{-1} to increase, consistent with the conversion of free O–H groups into O–H groups hydrogen-bonded to an acetone carbonyl group. At relatively low surface coverage—after 20 s of flow—the free OH groups on ice have largely vanished; this does not occur until a higher relative surface coverage on water. This again points to a different mode of adsorption on the different surfaces.

The fit results were also used to analyze the shift of the hydrogen-bonded O–H stretching modes, as illustrated for acetone/ice and acetone/water in Figure 3 e and Figure 3 f, respectively. For the ice surface, a red-shift of about 20 cm^{-1} was observed following acetone adsorption whereas the water surface demonstrated, if anything, a blue-shift.

The blue-shift of the O–H stretching vibration of water upon addition of acetone has also been observed in bulk water by infrared absorption experiments.[25,33] Experimental and theoretical studies have concluded that the addition of acetone to water tends to "segregate" the water by forming water–water and acetone–acetone clusters.[34,35] However, at the water surface, the shift in the low-frequency hydrogen-bonded OH band could be due to intermolecular coupling,[36] and the binding of acetone to a free OH group will also affect the frequency of the other OH group in the same water molecule. Therefore, different factors could contribute to the shift of the low-frequency O–H stretching mode, but the opposite shifts observed for ice and water seem to indicate opposite effects of the presence of acetone on the interfacial hydrogen-bonded structure. The opposing shift in the O–H stretching mode upon addition of acetone to water and ice surfaces can play a direct role in photochemical reactions via vibrational overtone pumping.[10,11] The overall difference between the fundamental O–H stretching mode of the acetone/ice and acetone/water surfaces is approximately 40 cm^{-1}; this change would be even more pronounced in the overtone region as the overtone is roughly two times the fundamental frequency.

In conclusion, we have demonstrated the direct measurement of vapor-deposited acetone molecules on an ice surface by SFG spectroscopy. Such controlled-flow experiments enable the study of a plethora of small-molecule interactions with ice surfaces. The results for acetone reveal marked differences between acetone adsorption on ice and water surfaces. Upon adsorption of acetone on the ice surface, interaction primarily occurs between acetone and the free O–H groups, increasing the strength of interfacial water–water hydrogen bonds; for liquid water, the interaction seems less specific and leads to an overall weakening of the interfacial water hydrogen bonds.

Experimental Section

Materials

Acetone (99.98%) was purchased from Fisher Scientific. Millipore H_2O (Resistivity 18.2 Ω cm) was used for ice growth and the water samples.

Sample preparation

Single-crystalline, hexagonal ice (Ih) was grown by seed extraction from a melt. A seed, approximately $40 \times 40 \times 10$ mm^3, was frozen to a copper pin. Next, a molten layer over the entire surface of the seed was produced using a heat gun. The seed was partly submerged into the melt (Millipore water), which was set to 0.2 °C with a chiller (Thermo Scientific PC 200). After 1 h, the ice crystal was extracted from the melt at a rate of about 1.3 mm h^{-1}. The ice boule was harvested after about 24 h and stored at −20 °C. A Rigsby stage was used to check the crystallinity of the sample, and Formvar etching was used to check the orientation. All ice samples were oriented to the basal plane. The ice boule was sliced with a bandsaw to a 5 mm thick sample. A 44 mm aluminum circular cutter was used to produce ice samples of reproducible size. The ice slice was melted to the pin in the center of the sample cell at +7 °C and then cooled down to −20 °C. The sample cell was cleaned in acetone, ethanol, and Millipore water and sonicated in each solvent for 15 min. The sample cell was thoroughly rinsed with Millipore water and put on a hot plate to remove any remaining solvents. The ice sample was microtomed with a disposable microtome blade (Leica Surgipath) to be 4 mm thick. The sample cell was closed with a CaF_2 window and a threaded lid to ensure an airtight seal. The sample was kept at −20 °C overnight for annealing.

SFG spectroscopy

The experimental setup was based on a 1 kHz Ti:Sapphire regenerative amplifier (Spectra-Physics Spitfire Pro), which generates ca. 40 fs pulses centered at 800 nm and ca. 5 mJ in energy. Part of the 800 nm output was directed to a commercial optical parametric amplifier (TOPAS-C, Light Conversion) with a subsequent DFG crystal ($AgGaS_2$) to produce mid-infrared pulses centered at 3000 cm^{-1}, 11 μJ in energy and with a FWHM of about 400 cm^{-1}. Another portion of the 800 nm output was spectrally narrowed to 20 cm^{-1} with a Fabry–Perot etalon. The incident angles were 30° and 55° with respect to the surface normal for the visible and IR beams, respectively. The IR energy at the sample was reduced to 2 μJ to avoid melting the ice. The SFG signal was focused onto a spectrograph (Acton SP-300i, Princeton Instruments) and detected on a CCD camera (Newton 971 Andor). All spectra were collected in *ssp* polarization combination (*s*-polarized SFG, *s*-polarized visible, and *p*-polarized IR). A background, measured with the IR beam blocked, was subtracted from all spectra, and the data were subsequently normalized to the nonresonant signal from *z*-cut quartz.

For the SFG experiments on ice, the ice sample was cooled to −30 °C with a chiller (Lauda). A homebuilt sample cell (Figure 1 in the manuscript) was made out of perfluoroalkoxyalkanes (PFA) with a copper base and center. The sample cell constantly moved in an imperfect circular motion on the copper plated stage at a speed of 120 mm s^{-1}. The 1 mm offset for the circular motion allowed for more surface area to be probed. The flow experiments were completed by passing cooled nitrogen gas through PFA tubing into the cell at a rate of 2 L h^{-1} for 30 min. The stability of the sample was determined by turning the flow off and measuring the SFG signal for 15 min; no change was observed. This procedure was repeated twice. Next, 50 μL of acetone were added to a glass container that was chilled to about 0 °C. Cooled nitrogen was passed through the glassware with acetone and acted as a carrier gas to pass the acetone to the sample. The flow was turned off after certain exposure times to the acetone, and five spectra were collected with acquisition times of 1 min for the spectral region from 2800 to 3300 cm^{-1} and 3 min for the spectral region from 3400 to 3800 cm^{-1}. The five spectra were averaged to give the resulting spectrum for each flow time presented in Figure 2.

For the SFG experiments on water and acetone solutions, the samples were cooled to 0 °C. The sample cell for the water experiments was similar to the ice experiments with the exception of a small Teflon dish inside the cell to contain the solutions. The solutions were pipetted into the Teflon dish, and the cell was sealed with a CaF_2 window and a threaded lid. The spectra were acquired for 10 min.

Acknowledgements

We thank Yuki Nagata for helpful comments on the manuscript, John N. Crowley and Jos Lelieveld for fruitful discussions, and the MaxWater Initiative for financial support. J.D.C. thanks the Alexander von Humboldt Foundation for generous support.

Conflict of interest

The authors declare no conflict of interest.

Keywords: adsorption · ice surfaces · sum frequency generation spectroscopy · trace gases

How to cite: *Angew. Chem. Int. Ed.* **2019**, *58*, 3620–3624
Angew. Chem. **2019**, *131*, 3659–3663

[1] H. Singh, Y. Chen, A. Staudt, D. Jacob, D. Blake, B. Heikes, J. Snow, *Nature* **2001**, *410*, 1078–1081.
[2] L. Jaeglé et al., *J. Geophys. Res.-Atmos.* **2000**, *105*, 3877–3892; et al., *J. Geophys. Res.-Atmos.* **2000**, *105*, 3877–3892.
[3] J. E. Schaff, J. T. Roberts, *Langmuir* **1998**, *14*, 1478–1486.
[4] P. Behr, A. Terziyski, R. Zellner, *J. Phys. Chem. A* **2006**, *110*, 8098–8107.
[5] A. K. Winkler, N. S. Holmes, J. N. Crowley, *Phys. Chem. Chem. Phys.* **2002**, *4*, 5270–5275.
[6] M. Petitjean, M. Darvas, S. Picaud, P. Jedlovszky, S. L. Calvé, *ChemPhysChem* **2010**, *11*, 3921–3927.
[7] D. E. Starr, D. Pan, J. T. Newberg, M. Ammann, E. G. Wang, A. Michaelides, H. Bluhm, *Phys. Chem. Chem. Phys.* **2011**, *13*, 19988–19996.
[8] A. M. Grannas, A. R. Bausch, K. M. Mahanna, *J. Phys. Chem. A* **2007**, *111*, 11043–11049.
[9] T. F. Kahan, D. J. Donaldson, *J. Phys. Chem. A* **2007**, *111*, 1277–1285.
[10] D. J. Donaldson, A. F. Tuck, V. Vaida, *Chem. Rev.* **2003**, *103*, 4717–4730.
[11] V. Vaida, D. J. Donaldson, *Phys. Chem. Chem. Phys.* **2014**, *16*, 827–836.
[12] M. Staikova, M. Oh, D. J. Donaldson, *J. Phys. Chem. A* **2005**, *109*, 597–602.
[13] X. Wei, P. B. Miranda, Y. R. Shen, *Phys. Rev. Lett.* **2001**, *86*, 1554–1557.
[14] H. Groenzin, I. Li, V. Buch, M. J. Shultz, *J. Chem. Phys.* **2007**, *127*, 214502.
[15] M. A. Sánchez, T. Kling, T. Ishiyama, M.-J. van Zadel, P. J. Bisson, M. Mezger, M. N. Jochum, J. D. Cyran, W. J. Smit, H. J. Bakker, et al., *Proc. Natl. Acad. Sci. USA* **2017**, *114*, 227–232.
[16] W. J. Smit, F. Tang, Y. Nagata, M. A. Sánchez, T. Hasegawa, E. H. G. Backus, M. Bonn, H. J. Bakker, *J. Phys. Chem. Lett.* **2017**, *8*, 3656–3660.
[17] E. A. Raymond, T. L. Tarbuck, M. G. Brown, G. L. Richmond, *J. Phys. Chem. B* **2003**, *107*, 546–556.
[18] C. S. Tian, Y. R. Shen, *Chem. Phys. Lett.* **2009**, *470*, 1–6.

[19] S. Nihonyanagi, T. Ishiyama, T. Lee, S. Yamaguchi, M. Bonn, A. Morita, T. Tahara, *J. Am. Chem. Soc.* **2011**, *133*, 16875 – 16880.
[20] I. V. Stiopkin, C. Weeraman, P. A. Pieniazek, F. Y. Shalhout, J. L. Skinner, A. V. Benderskii, *Nature* **2011**, *474*, 192.
[21] H. C. Allen, E. A. Raymond, G. L. Richmond, *Curr. Opin. Colloid Interface Sci.* **2000**, *5*, 74 – 80.
[22] Y. L. Yeh, C. Zhang, H. Held, A. M. Mebel, X. Wei, S. H. Lin, Y. R. Shen, *J. Chem. Phys.* **2001**, *114*, 1837 – 1843.
[23] H. Chen, W. Gan, B. Wu, D. Wu, Z. Zhang, H. Wang, *Chem. Phys. Lett.* **2005**, *408*, 284 – 289.
[24] B. Morris, D. W. Davidson, *Can. J. Chem.* **1971**, *49*, 1243 – 1251.
[25] J.-J. Max, C. Chapados, *J. Chem. Phys.* **2003**, *119*, 5632 – 5643.
[26] J.-J. Max, C. Chapados, *J. Chem. Phys.* **2004**, *120*, 6625 – 6641.
[27] Y. Nagata, S. Mukamel, *J. Am. Chem. Soc.* **2010**, *132*, 6434 – 6442.
[28] T. Ohto, E. H. G. Backus, C.-S. Hsieh, M. Sulpizi, M. Bonn, Y. Nagata, *J. Phys. Chem. Lett.* **2015**, *6*, 4499 – 4503.
[29] Y. Nojima, Y. Suzuki, S. Yamaguchi, *J. Phys. Chem. C* **2017**, *121*, 2173 – 2180.
[30] Y. Nojima, Y. Suzuki, M. Takahashi, S. Yamaguchi, *J. Phys. Chem. Lett.* **2017**, *8*, 5031 – 5034.
[31] S. Nihonyanagi, S. Yamaguchi, T. Tahara, *J. Chem. Phys.* **2009**, *130*, 204704.
[32] J. Wang, P. J. Bisson, J. M. Marmolejos, M. J. Shultz, *J. Chem. Phys.* **2017**, *147*, 064201.
[33] S. Lotze, C. C. M. Groot, C. Vennehaug, H. J. Bakker, *J. Phys. Chem. B* **2015**, *119*, 5228 – 5239.
[34] S. E. McLain, A. K. Soper, A. Luzar, *J. Chem. Phys.* **2007**, *127*, 174515.
[35] D. S. Venables, C. A. Schmuttenmaer, *J. Chem. Phys.* **2000**, *113*, 11222 – 11236.
[36] J. Schaefer, E. H. G. Backus, Y. Nagata, M. Bonn, *J. Phys. Chem. Lett.* **2016**, *7*, 4591 – 4595.

Manuscript received: November 28, 2018
Accepted manuscript online: January 2, 2019
Version of record online: February 8, 2019

